ChemistryOpen

Research Article
doi.org/10.1002/open.202100282

Chemistry Europe
European Chemical Societies Publishing

www.chemistryopen.org

Preparation of Cerium-Bismuth Oxide Catalysts for Diesel Soot Oxidation Including Evaluation of an Automated Soot-Catalyst Contact Mode

Sabrina Christina Hebert and Klaus Stöwe*[a]

Cerium-bismuth oxides have emerged as promising candidates for Diesel soot oxidation. The catalysts are synthesized via automated co-precipitation methods. T_{50} values, where 50% of soot is oxidized, and the dynamic oxygen storage capacity (OSC_{dyn}) are used to compare the catalytic activity. The activity is measured by thermogravimetric methods. The synthesized catalysts are characterized through powder X-ray diffraction (PXRD), Raman spectroscopy, and specific surface area (S_{BET}) measurements. This work investigates the influence of the contact mode between soot and catalyst. The literature-known manual contact modes "loose", "tight", and "wet" are compared with our developed automated contact mode, using a dual asymmetric centrifuge. The rotation speed rs and mixing time t_M have been varied independently. Both factors influence the T_{50} value. A continuous transition from loose to tight contact mode with increasing rotation speed rs can be shown. Furthermore, the automated contact mode shows better reproducibility behavior compared to manual contact modes.

Introduction

The World Health Organization classifies Diesel soot as carcinogenic.[1] Diesel soot is suspected to cause lung or cardiovascular diseases.[2,3] Furthermore, Diesel soot influences the atmospheric visibility, soiling of buildings, the vegetation, or the climate due to its optical properties depending on particle size, shape, and composition.[4,5] Nevertheless, Diesel cars are popular because of more efficient engines, better fuel economy, and lower emissions of HC, CO, and CO_2. Contrary to gasoline engines, Diesel engines emit higher quantities of NO_x and the so-called soot. Both pollutants are restricted by vehicle emission standards.[6] Therefore, different exhaust gas post-treatment technologies are established. For example, Diesel particulate filters (DPF) remove soot from the exhaust gas stream.[7,8] Over time, the Diesel soot collected accumulates in the DPF. As a consequence, the backpressure of the exhaust gas post-treatment system rises and leads to higher fuel consumption because of filter regeneration processes or even to filter failure.[9,10] In the event that the pressure threshold of the DPF is reached, the DPF has to be regenerated. Mainly, there are two regeneration approaches: active and passive regeneration.[11] During the passive regeneration process, the accumulated soot is continuously oxidized by a catalytic chemical reaction utilizing residual oxygen in the off-gas stream. In this regeneration mode, fuel penalty is minimized and no additional heat of the exhaust gas stream is needed. The disadvantage of the passive regeneration is the suitability, deactivation, and the catalysts costs. The catalysts used are most usually based on precious metals.[5,12,13] During the active regeneration process, there is a periodic combustion at temperatures of $T = 550\,^{\circ}C$ and higher of the accumulated soot in an oxidizing atmosphere. The required heat is generated by an electric heater, a flame-based burner, or microwave cavity.[14,15] Another possibility is the post-injection of fuel which is burnt in the Diesel oxidation catalyst to produce the heat for the Diesel soot combustion.[16] Catalyzed DPFs offer the possibility to lower the combustion temperature of soot to $T = 400\,^{\circ}C$ and overcome the problem of additional heat generation.[17] Different types of catalysts like spinels,[18–21] perovskites[22–26] or CeO_2-based catalysts[27–29] are investigated for soot oxidation. In this paper, co-precipitated cerium-bismuth oxides are used as catalysts for the combustion of the model Diesel soot, the commercial carbon black P90. Wolf reported that Bi-doped CeO_2 is a promising candidate for the Diesel soot oxidation.[30] Cui et al. synthesized Bi-doped CeO_2 using reverse strike co-precipitation methods. The soot oxidation occurred at tight and loose contact modes. Doping the CeO_2 lattice improves the lattice oxygen mobility. The best activity was reached by a catalyst of $Ce_{0.5}Bi_{0.5}O_x$ composition with $T_{50} = 324\,^{\circ}C$ at tight contact conditions.[31] Advantages of this system are the low costs and good availability of the precursors. In addition, the resulting catalysts are free of precious metals.[32] To test the catalytic activity in laboratory experiments instead of an engine test bench, the contact between soot and catalyst is crucial. There are several literature-known contact modes. Neeft et al. developed the "loose" and "tight" contact. The loose contact is determined by mixing soot and catalyst with a spatula for a preset time. The contact area between soot and catalyst is poor, resulting in high combustion temperatures. For the tight contact, soot and catalyst are milled in either an agate mortar or a ball mill for a preset time and, if necessary, rotation speed. This procedure increases the contact area between soot and catalyst.[33–35] Both contact modes involve manual steps

[a] S. C. Hebert, Prof. Dr. K. Stöwe
Department of Natural Science, Professorship of Chemical Technology
Chemnitz University of Technology
09111 Chemnitz (Germany)
E-mail: klaus.stoewe@chemie.tu-chemnitz.de

that influence the repeatability of the measurements. To overcome this problem, Hensgen et al. developed the "wet" contact. The wet contact is an intimate contact and determined by dispersing soot and catalyst in a dispersion agent. Acetone has proven to be the best candidate as dispersion agent. Hensgen et al. used nano-scaled CeO_2 as catalyst with different types of model soot. In their study, a good measurement repeatability was achieved.[36]

In the present paper, the loose, tight, and wet contact modes are compared using nano-scaled CeO_2 AdNanoCeria and co-precipitated CeO_2 and $Bi_{0.5}Ce_{0.5}O_x$ samples as catalysts. The catalysts are characterized using PXRD, Raman spectroscopy, XRF, S_{BET}, and OSC_{dyn} measurements. Furthermore, an automated contact mode with a dual asymmetric centrifuge is developed to exclude any manual influence using a commercial device. The T_{50} values serve to compare the activities measured by an automated serial thermogravimetric analysis method.

Results and Discussion

Catalyst Characterization

XRF measurements shown in Table 1 were performed to verify the nominal Bi and Ce percentages of the co-precipitated BiCeO samples (Bi:Ce = 1:1). The oxygen content is not included in the presented results because the detector does not allow the quantification of oxygen. The mass percentages of Bi and Ce of the BiCeO samples which are precipitated by the precipitants ammonium carbonate (AC) and oxalic acid (OA) differ not more than $\Delta m\% = 3\%$ between nominal and experimental received values.

Table 2 presents the results of the specific surface area S_{BET} and the dynamic oxygen storage capacity OSC_{dyn} measurements. S_{BET} was determined through N_2 physisorption experiments and by the multi-point BET method. The reference sample AdNanoCeria supplied by Evonik Degussa produced through flame spray pyrolysis has the highest $S_{BET} = 60\ m^2 \cdot g^{-1}$ and highest $OSC_{dyn} = 42\ \mu mol_{O_2} \cdot g_{cat}^{-1}$ compared to co-precipitated samples. The pure CeO_2 precipitated by AC solution has a lower $S_{BET} = 27\ m^2 \cdot g^{-1}$ as well as lower $OSC_{dyn} = 25\ \mu mol_{O_2} \cdot g_{cat}^{-1}$ compared to AdNanoCeria. In comparison, the pure CeO_2 precipitated by OA shows an even smaller specific surface with $S_{BET} = 4\ m^2 \cdot g^{-1}$. On the other hand, the standard deviation of the OSC_{dyn} relative to its absolute value of the CeO_2_OA is very high with $OSC_{dyn} = 5 \pm 4\ \mu mol_{O_2} \cdot g_{cat}^{-1}$ and implies an inhomogeneous sample with respect to the distribution of oxygen vacancies and redox ability. A reverse trend was shown by the BiCeO samples. The BiCeO_AC has a smaller surface area of $S_{BET} = 8\ m^2 \cdot g^{-1}$ compared to BiCeO_OA. On the contrary, the BiCeO precipitated by OA has a $S_{BET} = 15\ m^2 \cdot g^{-1}$, but the OSC_{dyn} is higher for BiCeO_AC compared to BiCeO_OA ($OSC_{dyn} = 25\ \mu mol_{O_2} \cdot g_{cat}^{-1}$ versus $OSC_{dyn} = 6\ \mu mol_{O_2} \cdot g_{cat}^{-1}$).

Table 1. Mass percentages m% of the co-precipitated BiCeO determined by standardless X-ray fluorescence (XRF) analysis. Shown are the averaged values of three repeated measurements of one sample at different points with standard deviations.

Composition of Oxide	Nominal Mass Percentage		Measured Mass Percentage	
	$m\%_{Ce}$	$m\%_{Bi}$	$m\%_{Ce}$	$m\%_{Bi}$
BiCeO_AC	42.49	57.51	45.52 ± 1.33	54.18 ± 1.64
BiCeO_OA	42.49	57.51	42.77 ± 0.47	56.33 ± 0.49

Table 2. Calculated specific surface areas according to Brunauer, Emmett, and Teller (S_{BET}) determined by nitrogen adsorption measurements. Calculated and averaged dynamic oxygen storage capacity (OSC_{dyn}) of two repeated measurements with standard deviation determined by TGA-DSC methods. Oxides are calcined at T = 800 °C.

System	S_{BET} [$m^2\,g^{-1}$]	OSC_{dyn} [$\mu mol_{O_2} \cdot g_{cat}^{-1}$]
AdNanoCeria	60.0	41.9 ± 0.7
CeO_2_AC	26.6	24.7 ± 2.0
BiCeO_AC	7.8	24.7 ± 4.6
CeO_2_OA	4.0	4.7 ± 4.1
BiCeO_OA	15.4	5.5 ± 0.1

PXRD and Raman Spectroscopy

Figure 1 shows the PXRD patterns of the reference sample AdNanoCeria and the co-precipitated samples. In general, the PXRD patterns of the samples precipitated by OA reveal higher FWHM (full width at half maximum) of the reflections compared to the samples precipitated by AC, especially for the sample BiCeO_OA indicating lower crystallite size. The samples AdNanoCeria, CeO_2_AC and CeO_2_OA crystallize in a cubic fluorite-type structure with space group $Fm\bar{3}m$. Table 3 presents the results of Rietveld refinements.

Both BiCeO samples consist of more than one crystalline phase. According to Rietveld refinements, the BiCeO_OA sample consists of three different crystalline phases with exclusive Bi^{3+} occupation on cation positions. These are the monoclinic α-Bi_2O_3 phase with space group $P2_1/c$, the tetragonal β-Bi_2O_3 phase with space group $P\bar{4}2_1c$, and the orthorhombic bismutite $Bi_2(CO_3)O_2$ phase with space group Imm2. For the BiCeO_AC sample, an amount of only m = 2.7 w% of bismutite is refined. Due to a detailed reflection profile analysis in the course of the Rietveld refinement, two cubic CeO_2 phases with different lattice parameters are identified in the BiCeO samples. One cubic fluorite-type phase is CeO_2 doped with Bi^{3+} and the other phase is pure CeO_2. This finding might be explained by the presence of domains of the CeO_2 phase with varying Bi^{3+} content due to substitution of Ce^{4+} by Bi^{3+}. The Bi^{3+}-doped CeO_2 phases in the samples BiCeO_AC and BiCeO_OA have larger lattice parameters a = 5.436(2) Å and a = 5.4237(3) Å compared to pure AdNanoCeria with a = 5.4082(1) Å. The substitution of Ce^{4+} by Bi^{3+} is accompanied by oxygen lattice defect formation of Frenkel-type as indicated by Equation (1) (in Kröger–Vink notation):

$$Bi_2O_3(CeO_2) \rightleftharpoons 2Bi'_{Ce} + V_O^{\cdot\cdot} + 3O_O^x \quad (1)$$

Figure 2 shows the Raman spectra of the oxides used or prepared in this work. AdNanoCeria, CeO_2_AC, and CeO_2_OA all reveal the typical band at $\nu = 462\ cm^{-1}$ which is the triply degenerate F_{2g} mode that corresponds to a symmetric Ce–O

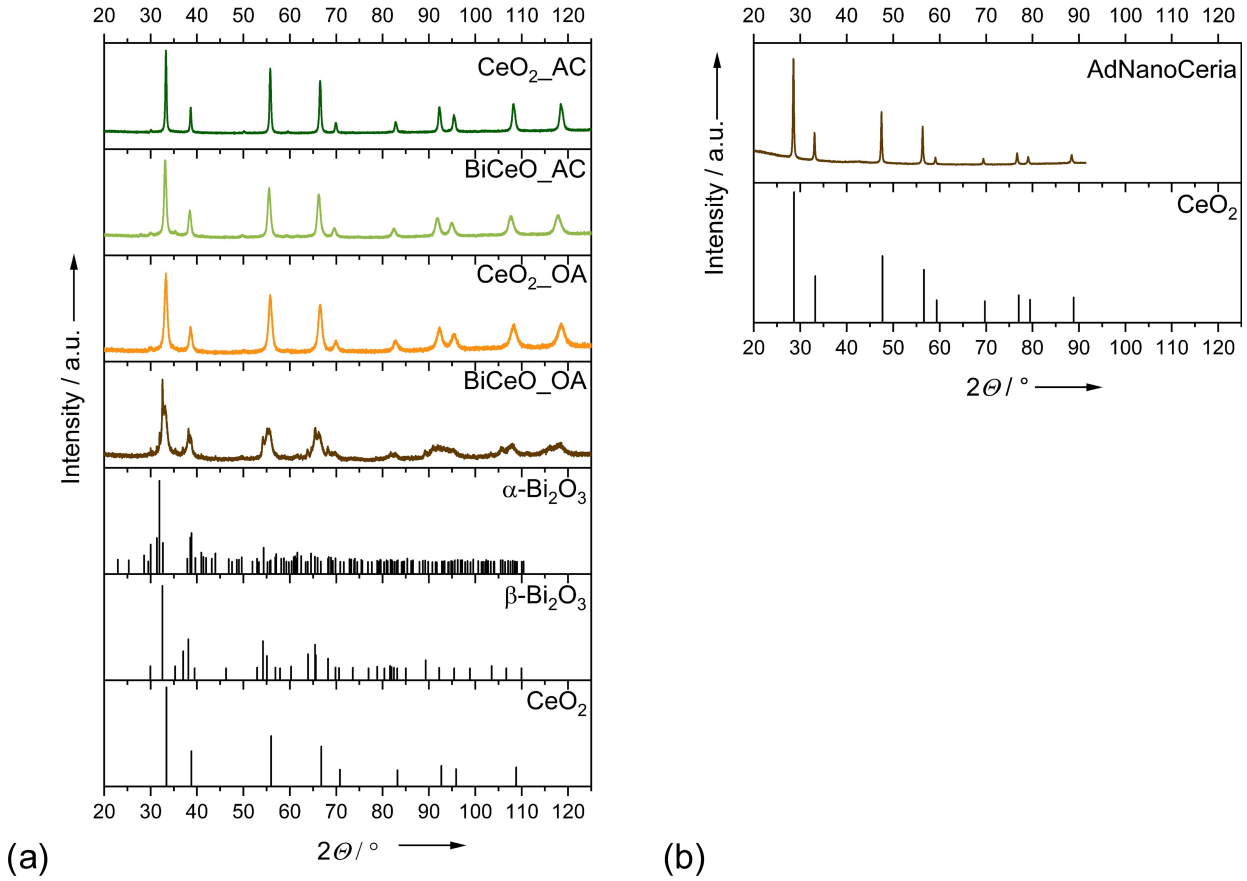

Figure 1. Powder X-ray diffraction (PXRD) pattern of co-precipitated BiCeO and CeO_2 with different precipitants and calcination at T = 800 °C as well as the reference sample AdNanoCeria. (a) PXRD measured with Co-K_α radiation, λ = 1.7892 Å. (b) PXRD measured with Cu-$K_{\alpha1}$ radiation, λ = 1.5406 Å. Following reference files are used: CeO_2: ICDD #75–76; α-Bi_2O_3: ICDD #71–2274; β-Bi_2O_3: ICDD #78–1793.

Table 3. Results of Rietveld refinement of the reference sample AdNanoCeria measured with Cu-$K_{\alpha1}$ radiation, λ = 1.5406 Å and the co-precipitated samples measured with Co-K_α radiation, λ = 1.7892 Å. Co-precipitated samples are calcined at T = 800 °C.

Sample	AdNanoCeria	CeO_2_AC	BiCeO_AC	CeO_2_OA	BiCeO_OA
CeO_2 [w%]	100	100	46(2)	100	62.1(12)
a [Å]	4.4082(1)	5.4109(5)	5.415(4)	5.4115(2)	5.4234(3)
Crystal size L [nm]	55.9(5)	46.5(2)	22.2(3)	15.2(1)	11.1(1)
$(Ce,Bi)O_2$ [w%]			51(2)		24(1)
a [Å]			5.436(2)		5.4929(5)
sof_{Ce} [%]			63.3(2)		60(7)
sof_{Bi} [%]			36.7(2)		40(7)
Crystal size L [nm]			26.2(4)		11.3(2)
$Bi_2(CO_3)O_2$ [w%]			2.7(1)		1.9(2)
a [Å]			5.47(3)		5.455(5)
b [Å]			27.4(1)		27.31(1)
c [Å]			5.45(5)		5.592(3)
Crystal size L [nm]			33(2)		34(4)
β-Bi_2O_3 [w%]					6.7(3)
a [Å]					7.7406(4)
c [Å]					5.6485(4)
Crystal size L [nm]					89(4)
α-Bi_2O_3 [w%]					5.0(5)
a [Å]					5.8494(5)
b [Å]					8.1632(6)
c [Å]					7.5106(7)
β [°]					112.995(7)
Crystal size L [nm]					330(60)
R_{WP}	4.190	5.068	4.939	5.820	6.237

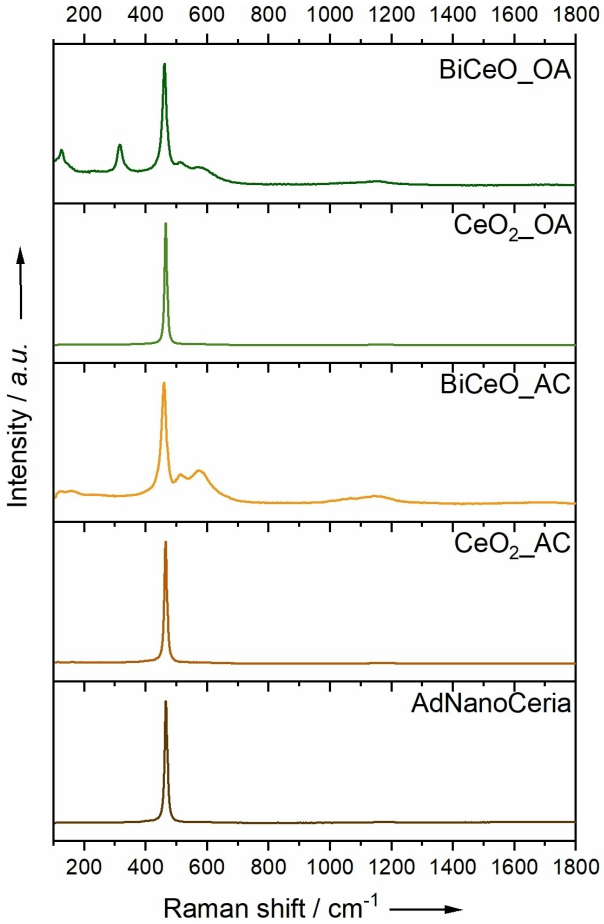

Figure 2. Raman spectra of the reference sample AdNanoCeria and the co-precipitated samples. Each sample was measured three times at different areas. Representative and, for the sake of comparison, normalized spectra are shown. Co-precipitated oxides are calcined at T = 800 °C. Laser wavelength is λ = 532 nm.

stretching vibration in the point group O_h representing the symmetric breathing mode of six O^{2-} anions around the central Ce^{4+} ion.[37,38] According to Schilling et al., two broad bands at $\nu = 510$ and 570 cm^{-1} can be assigned to oxygen vacancy formation of Frenkel-type $Ce^{3+}(O^{2-})_7V_O^{\cdot\cdot}$ and $Ce^{4+}(O^{2-})_7V_O^{\cdot\cdot}$.[37] As these bands are missing in the samples specified above, this confirms that all CeO_2 samples have nearly stoichiometric composition. The Raman spectrum of BiCeO_AC shows bands at $\nu = 121$, 161, 460, 514, 575, 1067, and 1148 cm^{-1}. The bands at $\nu = 121$, 161, and 1067 cm^{-1} can be assigned to bismutite[39] and confirm the results of Rietveld refinements. The band at $\nu = 460$ cm^{-1} can again be assigned to the F_{2g} band of CeO_2. The bands at $\nu = 514$ cm^{-1} and $\nu = 575$ cm^{-1} are broad and refer to the formation of the oxygen vacancies (see above) as a result of doping the CeO_2 lattice with Bi^{3+} ions (see Equation (1)) in consistence with the results of the Rietveld refinement. The broad band at $\nu = 1148$ cm^{-1} is referenced to the adsorption of oxygen molecules, which are adsorbed at the surface during the ex situ measurements due to contact with air forming O_2^{2-} groups at the surface by reaction with Ce^{3+} ions.[37] The Raman spectrum of the BiCeO_OA sample shows some other bands. These bands are observed at the frequencies $\nu = 126$, 229, 314, 460, 512, 575, and 1152 cm^{-1}. The bands at $\nu = 126$, 229, 314 cm^{-1} clearly refer to β-Bi_2O_3. Note that the band at $\nu = 460$ cm^{-1} can be assigned to both the F_{2g} mode of the CeO_2 lattice or β-Bi_2O_3.[40,41] Like in the Raman spectra for BiCeO_AC, there are the two broad bands at $\nu = 512$ and 575 cm^{-1} according to oxygen vacancies of the CeO_2 lattice. The band at $\nu = 1152$ cm^{-1} is again due to the vibration of O_2^{2-} group.[37] According to Bao et al., the intensity ratio I_{595}/I_{464} of the bands at $\nu = 464$ and 595 cm^{-1} is to be calculated to get a better comparison of the relative concentration of the defect complexes of the BiCeO samples.[42] The intensity ratio I_{595}/I_{464} of BiCeO_AC is 0.68(2) and that of BiCeO_OA amounts to 0.33(2). Therefore, the amount of defects in BiCeO_AC is higher than in BiCeO_OA.

Activity Measurements

Repeatability Behaviors of Different Contacts

The activity measurements are conducted with a serial thermogravimetric and differential scanning calorimetry system (TGA/DSC). The repeatability behaviors of the loose, tight, wet contact modes, and our development, the automated contact were investigated with nano-scaled AdNanoCeria, CeO_2_AC, and CeO_2_OA as sample materials. The samples are calcined at T = 800 °C to avoid any changes of the crystal structure during the reaction in a temperature range of T = 25–700 °C and to improve the crystallinity of the samples. Piumetti et al. investigated the influence of different CeO_2 crystal structures. They determined that calcination temperatures above T > 500 °C produces more active sites of the CeO_2 samples.[43] Hueso et al. showed that grinding their catalyst, a $L_{0.5}Sr_{0.5}CoO_{3-\delta}$ perovskite, and soot together can cause a partially reduction of Co^{3+} to Co^{2+}.[44] In the present investigation, we do not observe such an effect. Figure 3 shows the TGA curves measured for different contact modes between soot and catalyst with constant weight ratio of 1:4. AdNanoCeria60 was used for the activity measurements. Each gravimetric activity measurement was repeated five times. Considering Figure 3, loose and tight contact mode have problems of repeatability compared to wet and automated contact.

To compare the repeatability, the average and the standard deviation of the relative weight loss $\Delta m/m_0$ and $\sigma(m/m_0)$ can be used. The value $\Delta m/m_0$ should be close to $\Delta m/m_0 = 20\,\%$ (catalyst:soot = 4:1) and $\sigma(m/m_0)$ should be as low as possible. The obtained values are listed in Table 4. On the other hand, the T_{50} value is a good indicator of contact tightness: as the soot combustion is only occurring at the direct contact area between soot and catalysts, lower T_{50} values represent a more intimate contact between both components. The loose contact mode has the highest T_{50} value of $T_{50} = 631 \pm 6$ °C. On the other side, the automated contact possesses the lowest T_{50} value of $T_{50} = 436 \pm 2$ °C. The relative weight loss $\Delta m/m_0$ is in the same range of $\Delta m/m_0 \approx 21.5\,\%$ for all contact modes. The loose contact has the highest standard deviation of the relative

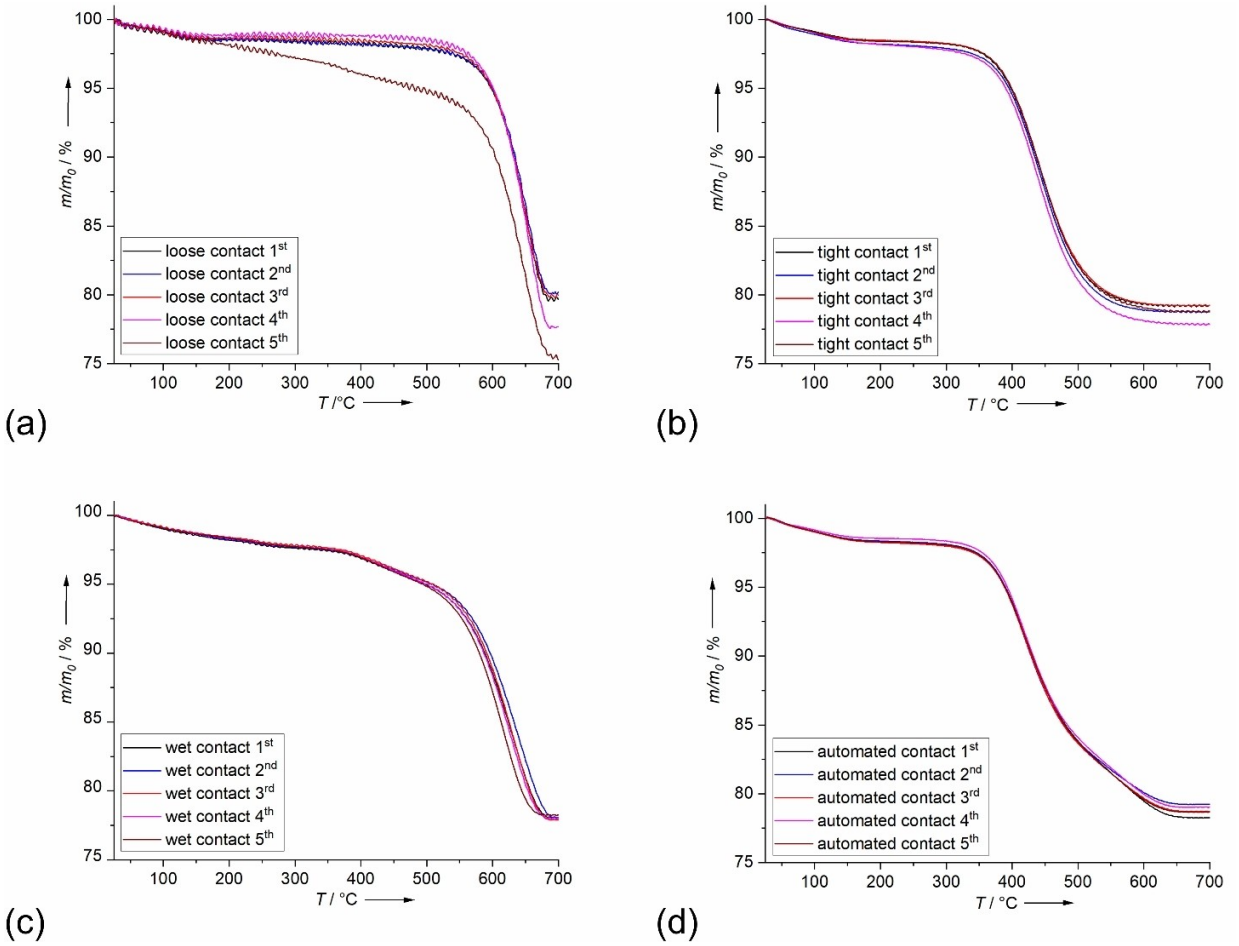

Figure 3. TGA curves of repeatability measurements of different contact modes between soot and AdNanoCeria60 as catalyst. Weight ratio between catalyst and soot is 4:1. Measurements are performed by a simultaneous TGA-DSC system with temperature range T = 25–700 °C and heating rate r = 5 °C·min^{-1} in synthetic air flow $\dot{V}$ = 25 mL·min^{-1}. The following contact modes are shown: (a) loose contact; (b) tight contact; (c) wet contact with dispersant acetone; and (d) automated contact realized by the dual asymmetric centrifuge at rotation speed rs = 3500 rpm and mixing time t_M = 300 s.

Table 4. T_{50} values and relative weight loss $\Delta m/m_0$ of soot during activity measurements determined by TGA measurements. AdNanoCeria was used as catalyst in a weight ratio of 4:1 of catalyst and soot. The averages and their standard deviations of five repeated measurements are shown. Automated contact realized by the dual asymmetric centrifuge at operating conditions rotation speed rs = 3500 rpm and mixing time t_M = 300 s. For additional measurements details, see the Experimental Section.

contact mode	T_{50} [°C]	$\Delta m/m_0$ [%]
loose	631.3 ± 5.6	21.5 ± 1.9
tight	439.0 ± 1.8	21.2 ± 0.5
wet	597.0 ± 5.6	21.9 ± 0.1
automated	436.1 ± 2.4	21.3 ± 0,3

Table 5. T_{50} values and relative weight loss $\Delta m/m_0$ of soot during activity measurements determined by TGA measurements. CeO_2_AC was used as catalyst in a weight ratio of 4:1 of catalyst and soot. The averages and their standard deviations of five repeated measurements are shown. Automated contact realized by the dual asymmetric centrifuge at rotation speed rs = 3500 rpm and mixing time t_M = 300 s.

Contact mode	T_{50} [°C]	$\Delta m/m_0$ [%]
Loose	652.1 ± 2.3	27.3 ± 11.8
Tight	625.8 ± 3.1	18.5 ± 0.1
Wet	621.2 ± 0.7	17.7 ± 2.8
Automated	631.7 ± 2.6	19.3 ± 4.1

weight loss with $\sigma(m/m_0) = 1.9\%$. The 5th repetition of this series (brown line) might be considered as an outlier, but is quite commonly observed for loose contact due to sample inhomogeneities (see below). This implicates that the loose contact has the lowest repeatability. The $\sigma(m/m_0)$ of the tight, wet, and automated contact are below $\sigma(m/m_0) = 1\%$. These values indicate good repeatability behavior.

In contrast to AdNanoCeria, for example CeO_2 precipitated by AC reveals different properties, see Figure 4 and Table 5. The loose contact mode shows a poor repeatability behavior and the highest T_{50} value with $T_{50} = 652 \pm 2$ °C. The average and deviation of the relative weight loss of soot is $\Delta m/m_0 = 27\%$ and $\sigma(m/m_0) = 12\%$. $\Delta m/m_0$ is approximately 7% higher than the theoretical relative weight loss of soot, indicating a rather inhomogeneous soot-catalyst mixture.

The wet contact mode seems to break into two different soot-catalyst mixtures, one mixture containing more and the other less soot. Compared to AdNanoCeria, CeO_2_AC might have a broad or even bimodal particle size distribution and

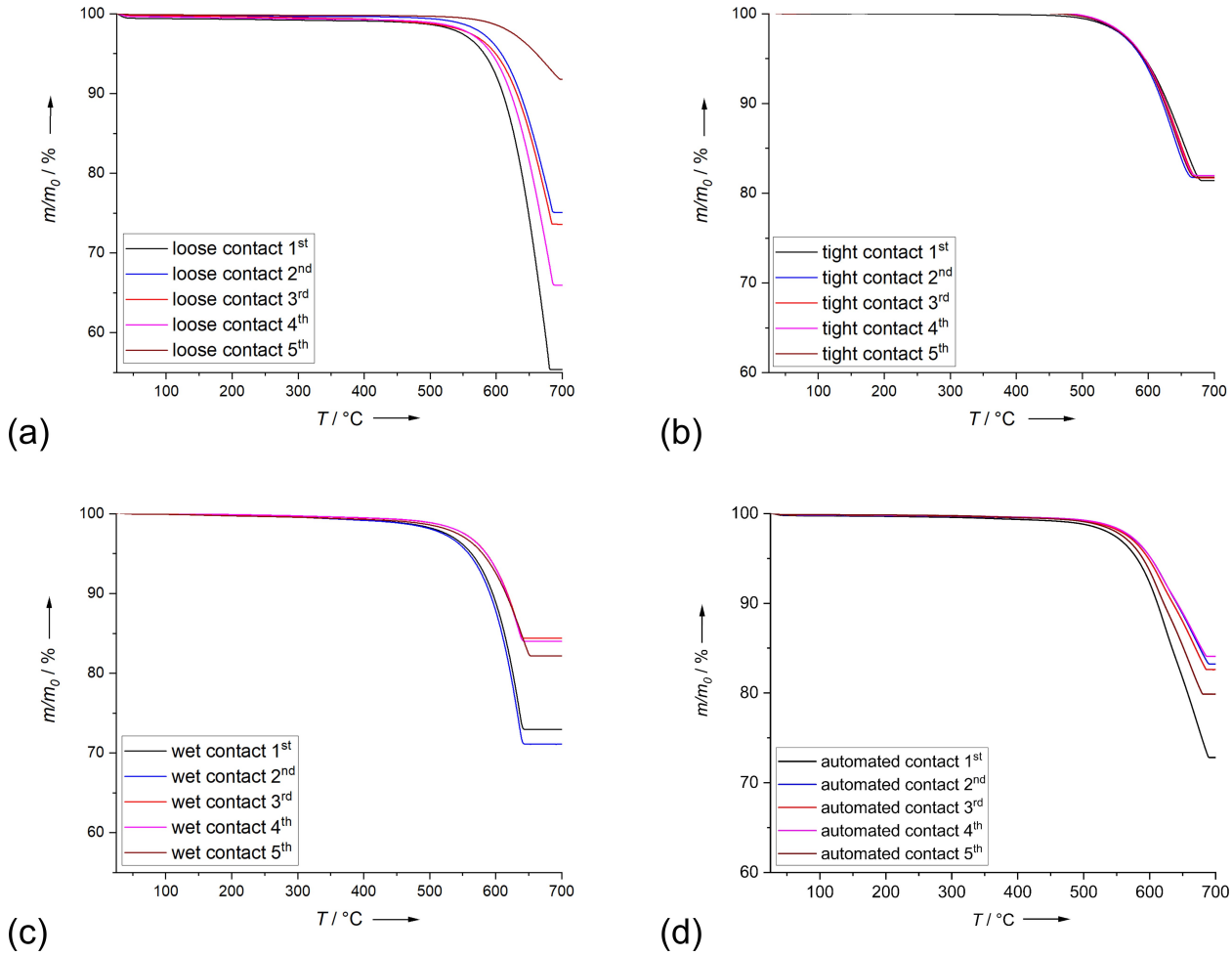

Figure 4. TGA curves of repeatability measurements of different contact modes between soot and CeO_2_AC as catalyst calcined at T = 800 °C. Weight ratio between catalyst and soot is 4:1. Measurements are performed by TGA-DSC system with temperature range T = 25–700 °C and heating rate r = 5 °C·min^{-1} in synthetic air flow $\dot{V}$ = 25 mL·min^{-1}. The following contact modes are shown: (a) loose contact; (b) tight contact; (c) wet contact with dispersion agent acetone; and (d) automated contact realized by the dual asymmetric centrifuge at operating conditions rotation speed rs = 3500 rpm and mixing time t_M = 300 s.

during the wet contact preparation despite intense stirring, there is a separation of particles of different size and thus also of the amount of soot connected to the catalyst's fractions. The tight contact has the lowest T_{50} value with $T_{50} = 621 \pm 1$ °C. The difference from the theoretical relative weight loss is quite low with $\Delta m/m_0 = 18.5 \pm 0.1$ %. The standard deviation is much smaller than 1 %, indicating good repeatability behavior as well as a homogeneous soot-catalyst mixture. The automated contact has a $T_{50} = 632 \pm 3$ °C, lying in between the loose and tight contact mode. As will be shown later, the automated mode offers the possibility to adjust the contact tightness by experimental parameters. The relative weight loss of soot is again quite close to the theoretical value with $\Delta m/m_0 = 19 \pm 4$ %. But the standard deviation of the relative weight loss is $\sigma(m/m_0) = 4$ % and thus higher than that of the tight contact mode, but better compared to the loose contact mode. As the automated contact is prepared by mixing soot and catalyst in a dual asymmetric centrifuge in polypropylene (PP) containers, which show different adhesion properties to the two components of the mixture, volume fractions of catalyst with soot-rich and -poor domains similar to those found for the wet contact mode might occur. In this case, also the sampling position (mixing container-wall near of close to center) has a certain influence on the sample properties.

Table 6 presents the results of T_{50} and $\Delta m/m_0$ measurements for the CeO_2_OA sample. It can be seen that the loose and wet contact mode have the highest T_{50} values with $T_{50,loose} = 651 \pm 1$ °C and $T_{50,wet} = 640 \pm 10$ °C. In this case, the

Table 6. T_{50} values and relative weight loss $\Delta m/m_0$ of soot during activity measurements determined by TGA measurements. CeO_2_OA was used as catalyst in a weight ratio of 4:1 of catalyst and soot. The averages and their standard deviations of five repeated measurements are shown. Automated contact realized by the dual asymmetric centrifuge at rotation speed rs = 3500 rpm and mixing time t_M = 300 s.

Contact mode	T_{50} [°C]	$\Delta m/m_0$ [%]
Loose	651.0 ± 1.3	20.7 ± 5.7
Tight	636.2 ± 2.0	20.3 ± 0.3
Wet	640.0 ± 9.6	26.6 ± 10.2
Automated	625.0 ± 3.1	17.9 ± 1.0

automated contact mode has the lowest $T_{50} = 625 \pm 3$ °C. With respect to repeatability behavior, the loose and wet contact mode have much higher standard deviations of the relative soot weight loss compared to the other two contact modes. This indicates homogeneous soot-catalyst mixtures and good repeatability behavior of tight and automated contact modes.

All in all, the automated contact shows good repeatability behavior according to the relative weight loss of soot. The T_{50} values achieved with the automated contact are in the range of the tight contact mode but the contact tightness can be adjusted by operational parameters as will be shown in the next chapter. It is noteworthy that the contact modes are influenced by specific properties of the samples and the fact that soot and catalyst have rather different surface polarities and energies. This makes the contact of the two components prone to demixing effects, additionally enforced by contact with accessories during the mixing process.

Further Investigation of the Automated Contact Mode

The automated contact was realized with a dual asymmetric centrifuge for a number of other samples, too. The investigation of operating conditions of the centrifuge are described in more detail in this section. The rotation speed rs was varied between rs = 300–3500 rpm in Δrs = 200 rpm steps and the mixing time was held constant at the two levels of $t_M = 60$ s and $t_M = 300$ s. The influence of rs at $t_M = 60$ s was investigated for all samples. The results are shown in Figure 5 and Table 7.

Based on the TGA curves and T_{50} values presented in Figure 5 and Table 7, there is a clear trend for all samples. With increasing rotation speed rs the TGA curves shift to lower temperatures and the T_{50} values decrease. The sample CeO_2_OA does not follow the trend of the other samples. Here, the problem is the low activity for soot oxidation due to both low S_{BET} and low OSC_{dyn}. The largest effect of increasing rs is seen for the AdNanoCeria60 sample in agreement with the by far highest S_{BET} and highest OSC_{dyn} within the samples investigated resulting in good activity for the soot oxidation reaction. For further explanation of the results, the particle size distributions measured by static light scattering were used, represented in Figure 6. The samples AdNanoCeria, CeO_2_AC and BiCeO_AC possess a broad particle size distribution. Especially, in the range of hydrodynamic diameter d_h below $d_h = 10$ µm there are more particles available in these samples. For the samples precipitated by oxalic acid, the particles are more narrowly distributed around the maximum hydrodynamic diameter of $d_h \approx 11$ µm and there are not many particles with sizes below $d_h = 10$ µm. Table 7 shows the T_{50} values at different rotation speeds. The highest difference of combustion temperature between the loose contact-like condition at rs = 300 rpm and the tight contact at rs = 3100 rpm is achieved by the nano-scaled AdNanoCeria60 with $\Delta T_{50} = 213$ °C. The shift of T_{50} values is greater for the samples precipitated by AC than for those precipitated by OA. The ΔT_{50} values of BiCeO_AC and CeO_2_AC are $\Delta T_{50} = 57$ °C and $\Delta T_{50} = 77$ °C, respectively. On the other hand, BiCeO_OA and CeO_2_OA have a shift of T_{50} values of only $\Delta T_{50} = 10$ °C and $\Delta T_{50} = 45$ °C to lower temperatures, respectively. Furthermore, the BiCeO_AC has, at the lowest rotation speed of rs = 300 rpm, the lowest T_{50} value of $T_{50} = 539 \pm 1$ °C, indicating the best activity towards soot oxidation at loose contact conditions.

In Figure 7, the T_{50} values of the samples used in this work are compared at different rotation speeds rs. As already described above, the nano-scaled AdNanoCeria60 has the greatest shift of T_{50} values and the lowest T_{50} value of $T_{50} = 394 \pm 1$ °C at rs = 3100 rpm. The BiCeO_AC shows the best catalytic activity of the precipitated samples with lowest T_{50} value of $T_{50} = 482 \pm 1$ °C at rs = 2100 rpm. The CeO_2_OA sample shows the lowest activity towards soot oxidation and the lowest ΔT_{50} value.

The next step was to investigate the influence of the mixing time t_M. Experiments are performed with the AdNanoCeria60 and the BiCeO_OA samples at two different mixing times of $t_M = 60$ s and 300 s. The resulting T_{50} values on variation of rs

Table 7. Averages of T_{50} values and their standard deviations of two repeated measurements determined by TGA in automated contact mode at different rotation speeds rs at constant mixing time $t_M = 60$ s with the dual asymmetric centrifuge. The lowest T_{50} values at the lowest rotation speed as well as the overall minimum at all rotation speeds are underlined.

	AdNanoCeria	CeO_2_AC	BiCeO_AC	CeO_2_OA	BiCeO_OA
rs [rpm]	$T_{50} \pm \sigma_{T50}$ [°C]	$T_{50} \pm \sigma_{T50}$ [°C]	$T_{50} \pm \sigma_{T50}$ [°C]	$T_{50} \pm \sigma_{T50}$ [°C]	$T_{50} \pm \sigma_{T50}$ [°C]
300	607.2 ± 2.0	632.0 ± 0.2	*539.0 ± 0.1*	641.3 ± 0.7	565.5 ± 0.4
500	606.1 ± 1.8	627.3 ± 0.6	512.4 ± 0.4	640.1 ± 0.2	558.3 ± 3.6
700	588.1 ± 1.5	622.8 ± 0.4	504.5 ± 0.8	639.0 ± 0.1	550.8 ± 0.1
900	574.1 ± 1.6	619.7 ± 0.2	499.6 ± 3.0	637.7 ± 0.1	546.5 ± 1.6
1100	545.3 ± 0.8	614.7 ± 1.6	492.1 ± 0.7	634.7 ± 0.1	534.7 ± 0.8
1300	521.8 ± 0.7	600.6 ± 1.7	492.3 ± 0.5	633.1 ± 0.1	529.2 ± 0.7
1500	518.8 ± 1.2	594.9 ± 0.2	488.4 ± 1.2	632.4 ± 0.1	530.4 ± 0.8
1700	480.0 ± 1.3	594.9 ± 3.6	485.6 ± 1.5	632.6 ± 1.5	533.6 ± 1.0
1900	457.0 ± 1.4	588.2 ± 1.1	481.9 ± 0.4	633.4 ± 0.7	529.5 ± 1.0
2100	433.5 ± 1.2	587.0 ± 1.1	481.7 ± 0.9	633.2 ± 0.4	526.7 ± 0.6
2300	416.3 ± 0.1	582.4 ± 0.6	483.2 ± 0.8	634.7 ± 1.3	526.4 ± 0.4
2500	404.7 ± 1.3	573.6 ± 0.8	485.7 ± 0.7	631.7 ± 1.0	523.7 ± 0.0
2700	402.8 ± 0.1	572.4 ± 2.3	489.3 ± 0.3	631.9 ± 0.5	524.0 ± 0.7
2900	403.6 ± 0.1	566.4 ± 2.3	485.0 ± 1.5	632.7 ± 0.1	522.9 ± 1.5
3100	*393.9 ± 0.1*	564.0 ± 2.6	484.7 ± 1.2	633.3 ± 0.8	520.4 ± 0.2
3300	396.7 ± 0.1	561.1 ± 0.2	489.5 ± 0.4	631.1 ± 0.5	521.9 ± 1.9
3500	402.9 ± 0.1	555.4 ± 2.6	490.0 ± 0.9	630.2 ± 0.8	523.5 ± 0.2

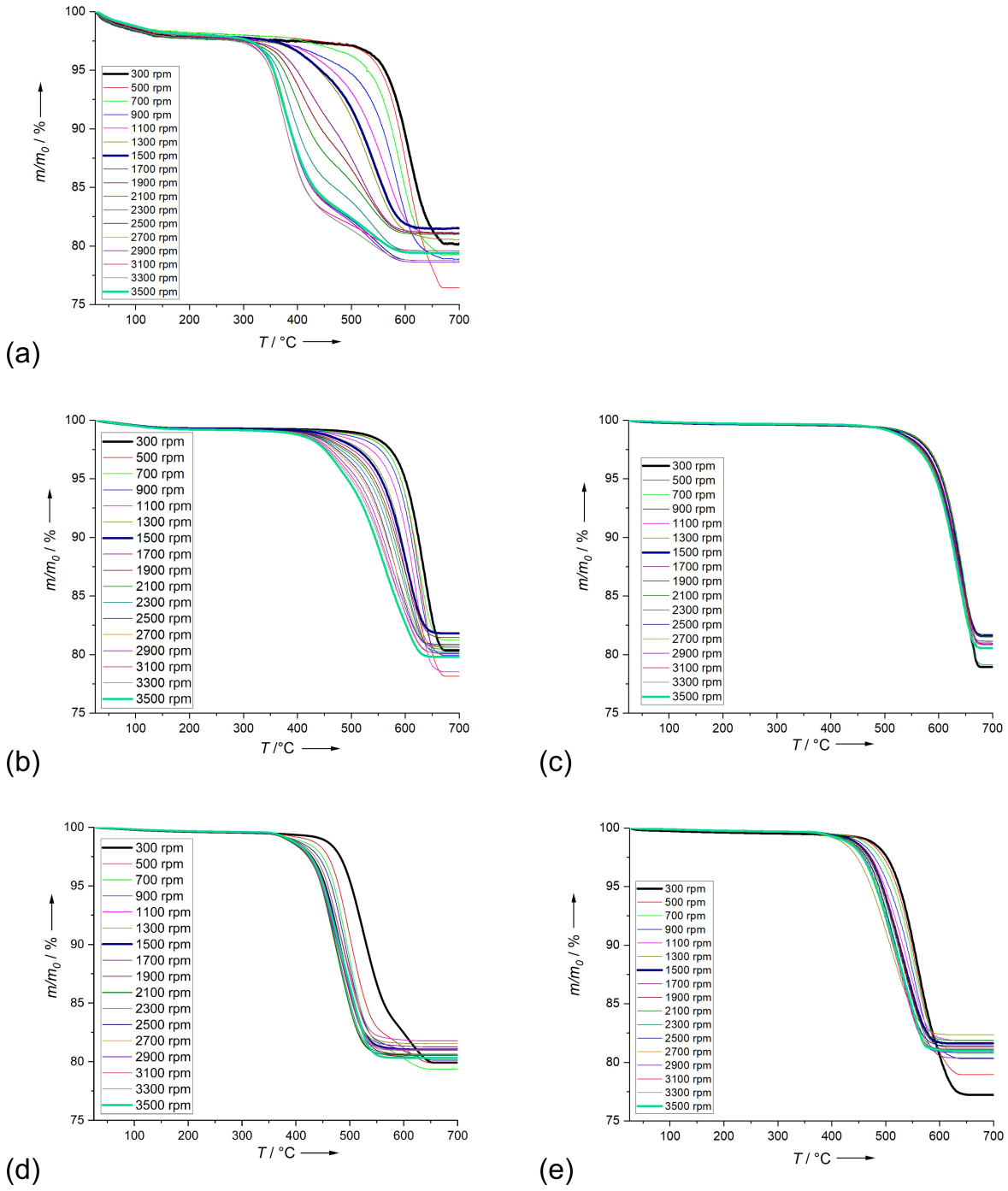

Figure 5. TGA curves from the investigation of the rotation speed rs for the automated contact mode. Measurements are performed by TGA-DSC system with temperature range T = 25–700 °C and heating rate r = 5 °C·min^{-1} in synthetic air flow $\dot{V}$ = 25 mL·min^{-1}. Catalyst-soot weight ratio is 4:1. Mixing time t_M = 60 s. The following catalysts are shown: (a) AdNanoCeria60; (b) CeO_2_AC; (c) CeO_2_OA; (d) BiCeO_AC; (e) BiCeO_OA.

are shown Figure 8 and Table 8. The influence of the mixing time t_M is not as large as that of the rotation speed rs. For the AdNanoCeria60, the mixing time t_M of 300 s decreases the T_{50} values. The difference of T_{50} values is not more than ΔT_{50} = 25 °C at rs = 1100 rpm. At rather high mixing rates of rs = 2700 rpm and above, the T_{50} differences decrease again to ΔT_{50} = 7 °C. Furthermore, the lowest T_{50} is observed at rs = 3000 rpm. Further increasing of rs leads to a small increase of T_{50} value. For the BiCeO_OA sample, the greatest difference between the T_{50} values is observed at a rotation speed rs of 3500 rpm with ΔT_{50} = 10 °C, indicating the minor influence of mixing time towards T_{50} values.

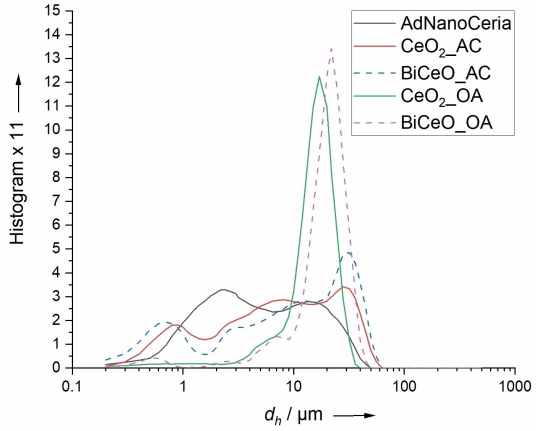

Figure 6. Histogram of the particle size distribution (PSD) of samples used in this work and determined by a static light scattering method. Five repeated measurements were recorded for each sample and all samples were treated with ultrasonic irradiation for t = 60 s before measurement. Every 5th measurement of the samples is shown.

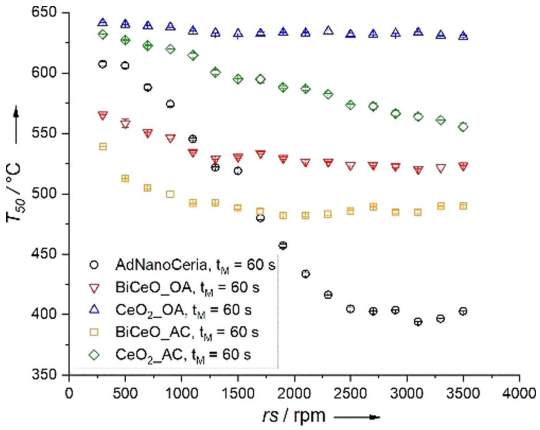

Figure 7. Comparison of soot oxidation T_{50} values and standard deviations of different catalysts in automated contact mode with mixing time $t_M = 60$ s. Measurements are performed by a TGA-DSC system in the temperature range T = 25–700 °C at a heating rate r = 5 °C·min^{-1} and a synthetic air flow $\dot{V} = 25$ mL·min^{-1}. Catalyst-soot weight ratio is 4:1.

Conclusion

In this article, the characterization of co-precipitated CeO_2 and 1:1 mixed bismuth-ceria oxides by PXRD, Raman analysis, XRF, S_{BET}, and OSC_{dyn} and a comparison of different contact modes between catalyst and soot known in literature for the catalytic oxidation of soot by temperature programmed oxidation methods have been described. Additionally, an automated contact mode realized by an asymmetric dual centrifuge has been investigated.

According to PXRD and Raman analysis, the AdNanoCeria60 and the co-precipitated CeO_2 samples crystallize in the cubic fluorite-type CeO_2 structure without any oxygen defects, that is, without non-stoichiometry in the ceria lattice. The two parameters S_{BET} and OSC_{dyn} are very low for the co-precipitated CeO_2 samples. Therefore, the activity for soot oxidation is lower compared to the AdNanoCeria60 sample which has the highest $S_{BET} = 60$ m^2·g^{-1} and $OSC_{dyn} = 42$ µmol$_{O_2}$·g$_{cat}^{-1}$ and, consequently, the highest soot combustion activity of the catalysts investigated in this study. The results of PXRD and Raman analysis show that the BiCeO_OA samples consist of four crystalline phases, namely α- and β-Bi_2O_3, bismutite $Bi_2(CO_3)O_2$, and a ceria phase with spatially inhomogeneous distribution of Bi^{3+} substitution for Ce^{4+} accompanied by oxygen lattice defects in the CeO_2 phase. The latter was modelled by two distinct CeO_2 phases in the Rietveld refinements with different site occupations factors sof(Bi^{3+}). In contrast, the BiCeO_AC sample only reveals the Bi^{3+}-doped CeO_2 phase together with a pure ceria phase and a small amount of bismutite. The OSC_{dyn} of BiCeO_AC is, with $\Delta OSC_{dyn} = 19$ µmol$_{O_2}$·g$_{cat}^{-1}$, higher than that of BiCeO_OA. Therefore, BiCeO_AC has a higher activity for soot oxidation than BiCeO_OA. Additionally, the Raman spectroscopy data show that the mixed oxides have Frenkel defects. The intensity ratio I_{595}/I_{464}, which is proportional to the concentration of defects, is higher for the BiCeO_AC sample compared to the BiCeO_OA sample. Additionally, the particle size distribution measured by static light scattering is broad for the samples precipitated by AC with high availability of particles with hydrodynamic diameter below $d_h = 10$ µm. The particles in the samples precipitated by OA are more narrowly distributed with a maximum hydrodynamic diameter $d_h = 11$ µm. This could be the reason for the better OSC_{dyn} and the better activity. The mixed oxides reveal better soot combustion activities compared to their pure CeO_2 samples recognizable by the lower T_{50} values.

Regarding to the investigation of different contact modes between soot and catalyst for different catalysts, the loose and wet contact mode show for all samples a low repeatability behavior. In marked contrast, tight and automated contact modes show good repeatability behavior. The automated contact has the advantage that there is no manual influence and is therefore not depending on the experimentator. Building on these results, the automated contact was further investigated. The rotation speed rs and the mixing time t_M were varied. The mixing time t_M has a much lower effect on the T_{50} values than the rotation speed rs.

Experimental Section

Catalyst Preparation

The chemicals listed below were used without further preparation. AdNanoCeria60 supplied by Evonik-Degussa with lot no. PH36701 and $S_{BET} = 60$ m^2·g^{-1} is used as reference material. All syntheses performed are described in detail in.[32]

Via co-precipitation, CeO_2 and the equimolar mixed oxide of cerium and bismuth are synthesized using the synthesis robot Accelerator SLT 106 from Chemspeed Technologies AG, Switzerland. Two precipitants are used: 1 mol $(NH_4)_2CO_3$ (food grade, BASF, abbreviated as AC) and 0.6 mol $C_2H_2O_4 \cdot 2\ H_2O$ (99%, ORG Laborchemie) dissolved in 1 L water (abbreviated as OA). The syntheses were performed in lined beakers with magnetic stirring bars. Using a thermostat from Huber Corp., the lined beakers were tempered to a temperature of T = 25 °C. The control of the thermostat was implemented in the "ApplicationExecutor" software for the syn-

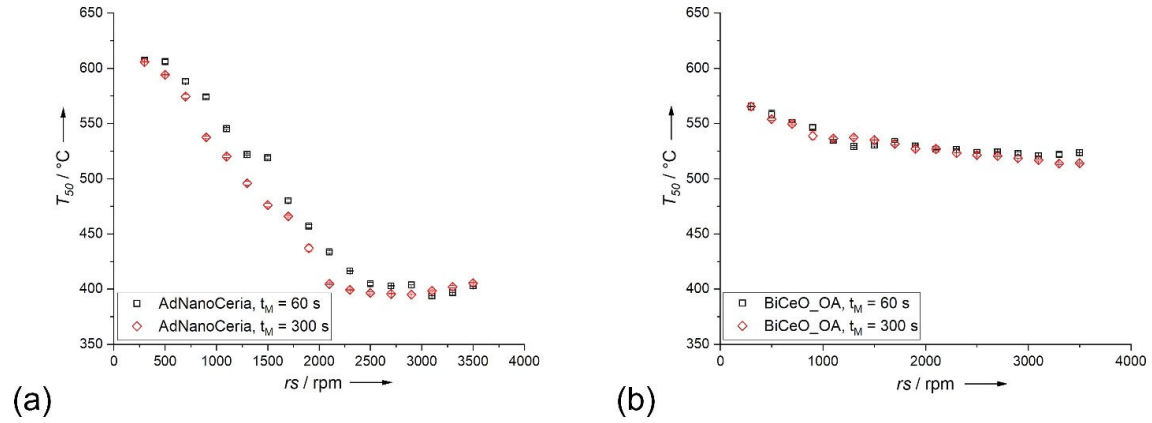

Figure 8. T_{50} values of soot oxidation for (a) AdNanoCeria60 and (b) BiCeO_OA in automated contact mode with varying rotation speeds rs at two mixing times $t_M = 60$ s and 300 s. Measurements are performed by TGA-DSC system with temperature range T = 25–700 °C and heating rate r = 5 °C·min^{-1} in synthetic air flow $\dot{V}$ = 25 mL·min^{-1}. Catalyst-soot weight ratio is 4:1.

Table 8. T_{50}-values of AdNanoCeria60 and BiCeO_OA measured at a TGA-DSC system in automated contact mode at different rotation speeds *rs* and mixing times $t_M = 60$ and 300 s.

	AdNanoCeria $t_M = 60$ s	AdNanoCeria $t_M = 300$ s	BiCeO_OA $t_M = 60$ s	BiCeO_OA $t_M = 300$ s
rs [rpm]	$T_{50} \pm \sigma_{T50}$ [°C]	$T_{50} \pm \sigma_{T50}$ [°C]	$T_{50} \pm \sigma_{T50}$ [°C]	$T_{50} \pm \sigma_{T50}$ [°C]
300	607.2 ± 2.0	605.7 ± 0.2	565.5 ± 0.4	565.5 ± 3.4
500	606.1 ± 1.8	594.1 ± 0.4	558.3 ± 3.6	553.9 ± 1.3
700	588.1 ± 1.5	574.4 ± 1.6	550.8 ± 0.1	549.7 ± 1.1
900	574.1 ± 1.6	537.4 ± 0.9	546.5 ± 1.6	538.9 ± 3.5
1100	545.3 ± 0.8	520.1 ± 0.9	534.7 ± 0.8	536.5 ± 1.1
1300	521.8 ± 0.7	495.9 ± 1.8	529.2 ± 0.7	537.3 ± 0.9
1500	518.8 ± 1.2	476.2 ± 1.6	530.4 ± 0.8	535.0 ± 0.1
1700	480.0 ± 1.3	465.9 ± 1.0	533.6 ± 1.0	531.7 ± 1.3
1900	457.0 ± 1.4	437.1 ± 2.8	529.5 ± 1.0	527.1 ± 1.4
2100	433.5 ± 1.2	404.6 ± 0.7	526.7 ± 0.6	526.8 ± 1.2
2300	416.3 ± 0.1	399.3 ± 0.7	526.4 ± 0.4	523.4 ± 0.1
2500	404.7 ± 1.3	396.6 ± 1.0	523.7 ± 0. 1	521.5 ± 1.3
2700	402.8 ± 0.1	395.6 ± 0.2	524.0 ± 0.7	520.6 ± 0.8
2900	403.6 ± 0.1	395.0 ± 0.1	522.9 ± 1.5	518.5 ± 0.1
3100	393.9 ± 0.1	398.6 ± 0.6	520.4 ± 0.2	516.8 ± 0.8
3300	396.7 ± 0.1	401.9 ± 1.0	521.9 ± 1.9	513.6 ± 0.7
3500	402.9 ± 0.1	405.3 ± 0.4	523.5 ± 0.2	514.2 ± 0.9

thesis robot. For the co-precipitation, 0.5 mol $Ce(NO_3)_3 \cdot 6\ H_2O$ and 0.5 mol $Bi(NO_3)_3 \cdot 5\ H_2O$ (99,5%, Alfa Aesar) were dissolved in 1 L of 1 mol·L^{-1} HNO_3 and transferred to beakers as reservoirs. With the help of the 4-needle head (4NH) of the synthesis robot, the volumes of the precursor solutions calculated were pipetted into lined beakers. For the mixed oxide $Bi_{0.5}Ce_{0.5}O_x$, abbreviated as BiCeO, equimolar amounts of the nitrate solutions are used. The precursors were mixed by magnetic stirring and kept at T = 25 °C. In different lined beakers, the two precipitants, which were dissolved in ultra-pure water, were also brought to the temperature T = 25 °C. The precipitants were transferred using the 4NH to the premixed and tempered nitrate solutions until the pH reached pH = 8 for AC and 3.5 times of the molar amount for OA was reached. The white to pale yellow precipitates were stirred for additional t = 0.5 h at T = 25 °C. The precipitates were filtered off from the supernatants through a 3-fold parallel pressure filtration station at an over-pressure of p = 1 bar after stirring. For filtration, Polyethersulfone membranes (Sartorius Stedim Biotech Corp.) with 0.1 µm mean pore size were used. The filtered-off samples were dried over night at room temperature, crushed and ground in an agate mortar until a fine powder was obtained and calcined at T = 800 °C for t = 5 h.

Table 9 summarizes the dispensing and aspirating speeds of the 4NH.

Contact between Soot and Catalyst

A weight ratio of 4:1 of catalyst and soot is used for all tests. The model soot used in this work is the carbon black P90 supplied by Evonik Degussa.

Table 9. Dispensing and aspirating speed of the pipetting steps. The 4-needle head (4NH) of the synthesis robot Chemspeed Accelerator SLT106 is used for liquid dosing.

Solution	Dispensing Speed [mL min^{-1}]	Aspirating Speed [mL min^{-1}]
0.5 mol L^{-1} $Ce(NO_3)_3$	40	40
0.5 mol L^{-1} $Bi(NO_3)_3$	40	40
1 mol L^{-1} $(NH_4)_2CO_3$	40	80
0.6 mol L^{-1} $C_2H_2O_4$	40	80

Loose Contact

Mixing soot and catalyst with a spatula for t = 60 s in a 5 mL glass vessel.

Tight Contact

Mixing soot and catalyst manually in an agate mortar for $t = 300$ s.

Wet Contact

Mixing soot and catalyst in acetone for t = 2.5 h in a 5 mL glass vessel under stirring. Afterwards, the suspension is dried for t = 48 h at T = 80 °C in order to get rid of acetone.

Automated Contact

The automated contact was performed using a dual asymmetric centrifuge Speedmixer™ DAC 150 from Hauschild Corp. Soot and catalyst are mixed in cups PP5–6 mL and the holder for a single sample was used. Experiments are performed at mixing times t_M = 60 s and 300 s. The rotation speed rs is varied in Δrs = 200 rpm steps between rs = 300 and 3500 rpm.

Activity Measurements

The activity measurements in means of T_{50} values and dynamic oxygen storage capacity OSC_{dyn} were investigated by automated serial thermogravimetric analyses coupled with heat flow differential scanning calorimetry (TGA-DSC 1 1600 from Mettler Toledo Corp.) according to Ref. [32]. Catalysts calcined at T = 800 °C were used for activity measurements. The T_{50} value is the temperature where 50 % of the soot mass is oxidized. To determine the T_{50} values, approximately m = 10 mg of the catalyst-soot mixture in a 4:1 weight-ratio was placed in a corundum crucible of volume V = 70 µL and heated to a temperature of T = 700 °C at a heating rate of r = 5 °C·min^{-1} with a synthetic air flow rate of $\dot{V}$ = 25 mL·min^{-1}. The T_{50} values were determined using the software Star^e (Mettler Toledo Corp.).

The dynamic oxygen storage capacity OSC_{dyn} is another significant property for soot oxidation catalysts. The OSC_{dyn} was determined experimentally with the TGA-DSC 1 1600 from Mettler Toledo Corp. already described. Two heating and cooling cycles were performed in order to calculate the OSC_{dyn}. Approximately m = 30 mg of the catalyst was placed in a V = 70 µL corundum crucible and heated to T = 700 °C under nitrogen flow of $\dot{V}$ = 25 mL·min^{-1} to get rid of adsorbed oxygen, water, or other compounds. The system was stabilized for t = 10 min. Afterwards, the system was cooled to T = 150 °C under synthetic air flow of $\dot{V}$ = 25 mL·min^{-1} for oxygen uptake and then stabilized for t = 10 min. This procedure was repeated and the weight loss of the second heating step was used for calculating the OSC_{dyn} as mass difference of $\frac{m_{O_2}^{150\,^\circ C} - m_{N_2}^{700\,^\circ C}}{M_{O_2} \cdot m_{cat}}$. The formula symbols have the following meaning: $m_{O_2}^{150\,^\circ C}$ is the mass of catalyst at a temperature of T = 150 °C after oxygen uptake, $m_{N_2}^{700\,^\circ C}$ is the mass of catalyst at T = 700 °C after oxygen release, M_{O_2} is the molar mass of oxygen, and m_{cat} is the buoyancy-corrected mass catalyst weighed in a V = 70 µL corundum crucible after desorption of compounds such as water. OSC_{dyn} is given in $\mu mol_{O_2} \cdot g_{cat}^{-1}$. The heating/cooling rate of r = 5 °C·min^{-1} was used for TGA-DSC measurements.

Catalyst Characterization

Powder X-Ray diffraction (PXRD) was performed on a Bruker D8 diffractometer with Co fine focus X-ray source (Ni filter, $\lambda_{K\alpha=}$ 1.79021 Å, Θ–Θ geometry, VDS, Lynxeye detector) for the co-precipitated samples. For the reference sample AdNanoCeria, the diffractometer STOE-Stadi P with Cu fine focus X-ray source (monochromator, $\lambda_{K\alpha1=}$1.54056 Å, Θ–Θ geometry, MYTHEN2 R1 K detector) was used. The intensity data were collected in the 2θ range from 20–125°. Qualitative phase identification was achieved by diffraction pattern assignment according to ICDD (International Centre for Diffraction Data) data as specified. Crystalline phases were identified through Rietveld refinement using the software TOPAS version 4.2 according to Refs. [45–47], which was adapted for the cerium-bismuth mixed oxides. Instrumental parameters for the fundamental parameter TOPAS refinement have been determined by refining a LaB_6 diffraction pattern as reference sample.

Raman spectra were measured with an inVia Raman Microscope (Renishaw Corp.). A frequency-doubled Nd:YAG laser of the model RL473 C from Renishaw with a wavelength of λ = 532 nm and a UVDD-CCD-Array detector with a grid consisting of 1800 lines/mm was used. Normally, laser powers of 0.5 % of the maximal laser power P = 50 mW and a measuring time of t = 60 s were employed. The calcined samples were placed on a 96-well microplate with V-shaped bottom (Greiner Corp.). The operating status of the microscope was line focus. Each sample was measured at three different points.

The determination of the specific surface according to Brunauer, Emmett and Teller was measured on a NOVA touch LX4 surface area & pore size analyzer (Quantachrome Corp.). The evaluation was performed with the software TouchWin™ version 1.11 (Quantachrome Corp.). The specific surface was measured by N_2 adsorption-desorption isotherms at the temperature of liquid N_2 with T = −196 °C. In preparation for the measurements, the samples were degassed under high vacuum for t = 4 h at T = 250 °C. The seven-point multi-point BET method was used to determine the specific surface S_{BET} in a relative pressure range of 0.02–0.25.

To determine the mass fractions of Bi and Ce, Energy-dispersive X-ray fluorescence (XRF) analyses were performed on a Fischerscope® X-RAY XAN® instrument and the evaluations with the software WinFTM® (Fischer Corp.). For the measurements, an excitation voltage of U = 30 keV and a measuring time of t = 60 s were used. The calcined catalysts were placed on top of a cellulose foil. Three repeated measurements were made at different locations on the sample and the composition average was taken. Calibration of the measurement data was performed using a standardless fundamental parameter method supplied by Fischer Corp. More details are described in Refs. [48–51].

Particle size distribution was measured by static light scattering performed on a CILAS 930 particle size analyzer. The range of hydrodynamic diameter was between d_h = 0.2–500 µm. Approximately m = 0.5 g of the catalysts were suspended in the water container of the analyzer at T = 25 °C and ambient pressure. In preparation of the particle size measurement, the samples dispersed in water were treated with ultrasound for t = 60 s to destroy agglomerates. This procedure was repeated for five times.

Author Contribution

S. C. H. built the experimental setups, performed experiments, analyzed data, and wrote this paper. K. S. supervised the work

and reviewed the article. All authors have read and agreed to the published version of the manuscript.

Acknowledgements

We thank the professorship for Coordination Chemistry (Prof. M. Mehring, M.Sc. I. Köwitsch) at TUC for measuring PXRD pattern and the professorship for Material and Surface Engineering (Prof. T. Lampke, M.Sc. Th. Mehner, M.Sc. M. Pügner, Dipl.-Ing. E. Benedix) at TUC for the possibility to measure XRF as well as PXRD pattern.

Conflict of Interest

The authors declare no conflict of interest.

Data Availability Statement

The data that support the findings of this study are available from the corresponding author upon reasonable request.

Keywords: automated catalyst soot contact · automated co-precipitation · catalyst soot contact · cerium-bismuth oxides · diesel soot oxidation

[1] WHO, in *J. Natl. Cancer Inst.*, **2012**, p. 1.
[2] M. M. Channell, M. L. Paffett, R. B. Devlin, M. C. Madden, M. J. Campen, *Toxicol. Sci.* **2012**, *127*, 179–186.
[3] P. E. Schwarze, A. I. Totlandsdal, M. Låg, M. Refsnes, J. A. Holme, J. Øvrevik, *BioMed Res. Int.* **2013**, *2013*, 685142.
[4] D. B. Kittelson, *J. Aerosol Sci.* **1998**, *29*, 575–588.
[5] R. Prasad, V. R. Bella, *Bull. Chem. React. Eng. Catal.* **2010**, *5*, 69–86.
[6] P. Tennison, C. Lambert, M. Levin, *SAE [Tech. Pap.]* **2004**, *113*, 573–579.
[7] T. V. Johnson, *SAE [Tech. Pap.]* **2001**, *1*, 68–81.
[8] T. V. Johnson, *Int. J. Engine Res.* **2009**, *10*, 275–285.
[9] J. Lupše, M. Campolo, A. Soldati, *Chem. Eng. Sci.* **2016**, *151*, 36–50.
[10] S. Iwasaki, T. Mizutani, Y. Miyairi, K. Yuuki, M. Makino, *SAE Int. J. Engines* **2011**, *4*, 527–536.
[11] K. Johansen, *Catal. Today* **2015**, *258*, 2–10.
[12] R. Matarrese, S. Morandi, L. Castoldi, P. Villa, L. Lietti, *Appl. Catal. B* **2017**, *201*, 318–330.
[13] K. Johansen, G. Mogensen, D. Mey, D. Pinturaud, *SAE Int. J. Fuels Lubr.* **2010**, *3*, 219–229.
[14] B. Zhang, J. E, J. Gong, W. Yuan, W. Zuo, Y. Li, J. Fu, *Appl. Energy* **2016**, *181*, 14–28.
[15] E. Jiaqiang, X. Zhao, L. Xie, B. Zhang, J. Chen, Q. Zuo, D. Han, W. Hu, Z. Zhang, *Energy* **2019**, *169*, 719–729.
[16] M. Zheng, S. Banerjee, *Appl. Therm. Eng.* **2009**, *29*, 3021–3035.
[17] M. Van Nieuwstadt, D. Upadhyay, M. Goebelbecker, W. Ruona, *SAE [Tech. Pap.]* **2003**, *112*, 48–55.
[18] M. Zawadzki, W. Walerczyk, F. E. López-Suárez, M. J. Illán-Gómez, A. Bueno-López, *Catal. Commun.* **2011**, *12*, 1238–1241.
[19] S. Zhang, X. Zhu, C. Zheng, D. Hu, J. Zhang, X. Gao, *Aerosol Air Quality Research.* **2017**, *17*, 2317–2327.
[20] K. Yoshida, S. Makino, S. Sumiya, G. Muramatsu, R. Helferich, *SAE [Tech. Pap.]* **1989**, *98*, 1994–2005.
[21] H. An, C. Kilroy, P. J. McGinn, *Catal. Today* **2004**, *98*, 423–429.
[22] Y. Teraoka, W. Shangguan, K. Jansson, M. Nygren, S. Kagawa, *Bull. Chem. Soc. Jpn.* **1999**, *72*, 133–137.
[23] Y. Teraoka, K. Kanada, S. Kagawa, *Appl. Catal. B* **2001**, *34*, 73–78.
[24] D. Fino, P. Fino, G. Saracco, V. Specchia, *Appl. Catal. B* **2003**, *43*, 243–259.
[25] Y. Teraoka, K. Nakano, W. Shangguan, S. Kagawa, *Catal. Today* **1996**, *27*, 107–113.
[26] Y. Teraoka, K. Nakano, S. Kagawa, W. F. Shangguan, *Appl. Catal. B* **1995**, *5*, L181–L185.
[27] G. Zhai, J. Wang, Z. Chen, S. Yang, Y. Men, *J. Hazard. Mater.* **2019**, *363*, 214–226.
[28] S. Yang, J. Wang, W. Chai, J. Zhu, Y. Men, *Catal. Sci. Technol.* **2019**, *9*, 1699–1709.
[29] J. Wang, L. Cheng, W. An, J. Xu, Y. Men, *Catal. Sci. Technol.* **2016**, *6*, 7342–7350.
[30] V. Wolf, **2015**. PhD Thesis, Universität des Saarlandes.
[31] B. Cui, Y. Li, S. Li, Y. Xia, Z. Zheng, Y. Q. Liu, *Energy Fuels* **2020**, *34*, 9932–9939.
[32] S. C. Hebert, K. Stöwe, *Materials* **2020**, *13*, 1369.
[33] J. Neeft, M. Makkee, J. Moulijn, *Appl. Catal. B* **1996**, *8*, 57–78.
[34] J. P. a Neeft, O. P. Van Pruissen, M. Makkee, J. a Moulijn, *Appl. Catal. B* **1997**, *12*, 21–31.
[35] J. P. a Neeft, M. Makkee, J. a Moulijn, *Chem. Eng. J.* **1996**, *64*, 295–302.
[36] L. Hensgen, K. Stöwe, *Catal. Today* **2011**, *159*, 100–107.
[37] C. Schilling, A. Hofmann, C. Hess, M. V. Ganduglia-Pirovano, *J. Phys. Chem. C* **2017**, *121*, 20834–20849.
[38] A. Nakajima, A. Yoshihara, M. Ishigame, *Phys. Rev. B* **1994**, *50*, 13297–13307.
[39] P. Taylor, S. Sunder, V. J. Lopata, *Can. J. Chem.* **1984**, *62*, 2863–2873.
[40] T. Selvamani, S. Anandan, L. Granone, D. W. Bahnemann, M. Ashokkumar, *Mater. Chem. Front.* **2018**, *2*, 1664–1673.
[41] A. J. Salazar-Pérez, M. A. Camacho-López, R. A. Morales-Luckie, V. Sánchez-Mendieta, F. Ureña-Núñez, *Superf. y vacío* **2005**, *18*, 4–8.
[42] H. Bao, X. Chen, J. Fang, Z. Jiang, W. Huang, *Catal. Lett.* **2008**, *125*, 160–167.
[43] M. Piumetti, S. Bensaid, N. Russo, D. Fino, *Appl. Catal. B* **2015**, *165*, 742–751.
[44] J. L. Hueso, A. Caballero, M. Ocaña, A. R. González-Elipe, *J. Catal.* **2008**, *257*, 334–344.
[45] R. W. Cheary, A. Coelho, *J. Appl. Crystallogr.* **1992**, *25*, 109–121.
[46] R. W. Cheary, A. A. Coelho, J. P. Cline, *J. Res. Natl. Inst. Stand. Technol.* **2004**, *109*, 1–25.
[47] A. Kern, A. A. Coelho, R. W. Cheary, in *Diffr. Anal. Microstruct. Mater.* (Eds.: E. J. Mittemeijer, P. Scardi), Springer Berlin Heidelberg, Berlin, Heidelberg, **2004**, pp. 17–50.
[48] D. Lagultton, W. Parrish, *Anal. Chem.* **1977**, *49*, 1152–1156.
[49] J. W. Criss, L. S. Birks, *Anal. Chem.* **1968**, *40*, 1080–1086.
[50] T. Shiraiwa, N. Fujino, *Jpn. J. Appl. Phys.* **1966**, *5*, 886–899.
[51] K. Ohno, J. Fujiwara, I. Morimoto, *X-Ray Spectrom.* **1980**, *9*, 138–142.

Manuscript received: December 7, 2021
Revised manuscript received: March 2, 2022